Pergamon

Acta mater. Vol. 47, No. 1, pp. 259–268, 1999
© 1998 Acta Metallurgica Inc.
Published by Elsevier Science Ltd. All rights reserved
Printed in Great Britain
PII: S1359-6454(98)00305-X
1359-6454/99 $19.00 + 0.00

A FUNCTIONALLY GRADED PARTICULATE COMPOSITE: PREPARATION, MEASUREMENTS AND FAILURE ANALYSIS

R. J. BUTCHER, C.-E. ROUSSEAU and H. V. TIPPUR†
Department of Mechanical Engineering, Auburn University, Auburn, AL 36849, U.S.A.

(Received 2 February 1998; accepted 25 August 1998)

Abstract—A functionally graded composite is prepared and the spatial gradation of Young's modulus in the functionally graded material (FGM) is measured. Elastic modulus gradients occur over length scales suitable for experimental mechanics investigations using optical interferometry. Crack tip fields are mapped in the FGM under quasi-static loading conditions with cracks oriented perpendicular to the direction of the elastic gradient and near the interface of the graded and the homogeneous portions of three-point-bending specimens. The optical measurements are used to extract fracture parameters based on the prevailing understanding of the crack tip behavior in FGMs. The results are also compared with finite element computations which incorporate measured elastic properties of the FGM. The advantage of using FGM interlayer as opposed to piecewise homogeneous joints is demonstrated through crack initiation tests. © *1998 Acta Metallurgica Inc. Published by Elsevier Science Ltd. All rights reserved.*

1. INTRODUCTION

Recent advances in materials processing and engineering have led to a new class of materials called functionally graded materials (FGMs). In these, dissimilar materials with contrasting thermo-mechanical properties are brought together to address the needs of aggressive environments of thermal shock and high strain rate loading. The primary difference between conventional cladding/bonding and the one using FGM interlayer is that in the latter the material properties are engineered to have a relatively smooth spatial variation unlike a step increase in the former thereby avoiding weak interfacial planes. Such materials have been developed using different processes including slip casting [1], centrifugal casting [2], laser alloying and cladding [3], and plasma-spray forming [4].

The FGMs pose new challenges in terms of modeling, characterization and optimization from the point of view of fracture behavior. The analytical work on modeling such materials, particularly fracture mechanics, goes back to the late 1970s. Atkinson and List [5] studied crack propagation in materials with spatially varying elastic constants. Gerasoulis and Srivastav [6] studied a Griffith crack problem in a nonhomogeneous medium using integral equation formulations. The critical importance of providing an accurate analysis for naturally occurring nonhomogeneities near material interfaces in real situations has been recognized in the works of Erdogan [7, 8]. Ozturk and Erdogan [9] performed a study of an axisymmetric problem with cracks oriented perpendicular to the direction of the nonhomogeneity. Their results suggest that this situation is less severe than the plane-strain counterpart in terms of stress intensity factors for identical nonhomogeneity constant. More recently, Chen and Erdogan [10] considered two homogeneous half-planes bonded through a nonhomogeneous layer with an exponential variation in elastic modulus perpendicular to the orientation of the crack. The lack of material symmetry and the configuration about the crack plane have led to mixed-mode deformations and cracks subjected to internal pressure are shown to experience significant mode-II deformation. Giannakopoulos *et al.* [11] investigated thermal stresses in functionally graded layered materials with compositional gradients. The influence of the architecture of the functionally graded coatings on thermally induced surface cracking in multilayer ceramic coatings is examined by Choules and Kokini [12]. Jin and Batra [13] discussed crack tip fields in general nonhomogeneous materials and examined crack growth resistance behavior using the rule of mixtures. Functionally graded metal/ceramic systems have been analyzed by Bao and Cai [14] to study fracture mechanics parameters as a function of coating gradation and crack location. The crack deflection in brittle FGMs is examined by Gu and Asaro [15] using the maximum energy release rate criterion.

It should be emphasized that at the moment experimental investigations on fracture behavior of

†To whom all correspondence should be addressed.

Table 1. Nominal bulk properties of the constituent materials

	E (GPa)	v	ρ (kg/m^3)
Epoxy	3.3	0.35	1150
A-glass	70.0	0.23	2200

FGMs is very limited. In this paper, the development of a functionally graded particulate composition using model materials is reported. The Young's modulus variation in the FGM is experimentally determined. The crack tip fields are optically mapped and measurement of fracture parameters based on prevailing analytical solutions is carried out. The measurements are compared with finite element computations which incorporate measured properties of the FGM. The failure performance of the FGM is examined relative to the piecewise-homogeneous and homogeneous specimens through fracture tests.

2. FGM PREPARATION AND MODULUS MEASUREMENT

A particulate composite with a continuously varying weight fraction of filler particles in a polymeric matrix was developed. Solid A-glass (soda-lime glass) spheres of mean diameter of 30 μm were used as filler material in a low viscosity, slow curing epoxy matrix. The nominal bulk elastic properties of the constituent materials are listed in Table 1. Rectangular strips of width 25 mm and thickness 6 mm were cast in acrylic molds and cured for 72 h at room temperature. The choice of spherical particles and slow curing at room temperature minimize residual stresses in the FGM. The gravity casting technique was used to obtain the continuously varying weight fraction, W_f ($W_f = w_g/(w_g + w_e)$), and w_g, w_e are the weight of the glass beads and epoxy in the mixture), along the length of the sample while it remains constant in the width and the thickness directions. A typical FGM sample, shown schematically in Fig. 1, consists of a rectangular strip whose ends have nearly constant weight fraction with an interlayer where the volume fraction of the filler material varies continuously over lengths ranging from 12.5 to 50 mm depending on the process variables. The two ends of the FGM will henceforth be referred to as epoxy-rich and glass-rich ends.

The Young's modulus was calibrated against ultrasonic pulse–echo measurements. The longitudinal wave speeds (C_l) were measured at discrete locations by launching ultrasonic pulses through the sample thickness and capturing the echo for measuring the time of flight of the incident pulse. A transducer with an active aperture of approximately 4 mm diameter was used to perform thickness average measurements in these cases. Since both the local Young's modulus and the average local density of the material vary along the length of the FGM, the measured values of C_l change continuously. A typical ultrasonic wave speed signature for an FGM sample along its length is plotted in Fig. 2. Evidently, in the epoxy-rich and glass-rich ends of the sample the wave speed measurements are nearly constant and approximately linear in the mid-section. *It should be emphasized that the choice of C_l as an indirect indicator of Young's modulus in this case is simply based on convenience and one could as well use other local measurements such as mean particulate spacing, microindentation response, weight/volume fraction, etc., if more convenient. Further, epoxy is a loading rate dependent material and hence the measurement of elastic properties under quasi-static conditions cannot be inferred directly by ultrasonic measurements since they provide only dynamic values.*

In order to use this data to determine the values of Young's modulus $E(y)$, *homogeneous* strips with different but constant weight fractions were *separately* cast and wave speeds were measured in them. A plot of the wave speed and the corresponding weight fraction used in preparing each of these samples is shown in Fig. 3(a). The relationship between the two parameters is nearly parabolic. These *homogeneous* strips were then studied using quasi-static cantilever beam deflection tests by subjecting them to tip loading (2 mm/min). The Young's modulus of the beam material under *quasi-static* loading conditions (E_{static}) was determined *independently* by measuring the load and the corresponding beam deflection and using the elementary beam deflection theory. A plot of the measured Young's modulus E_{static} and the weight fraction of the composition is shown in Fig. 3(b). The relationship between the modulus measurements and the wave speed in the corresponding homogeneous samples is also parabolic. Next, the average density (ρ) of each of the homogeneous beam samples was determined by measuring its volume and mass. A plot of the density of each of the beams as a function of its weight fraction is shown in Fig. 3(c).

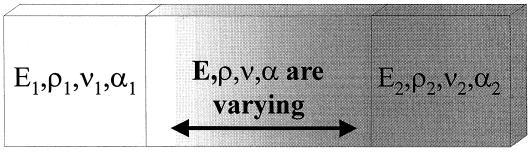

Fig. 1. Schematic of a functionally graded strip.

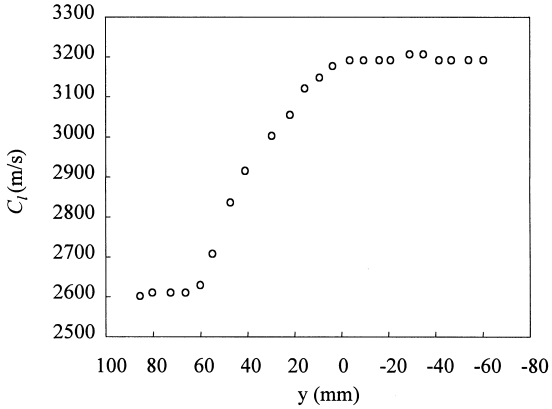

Fig. 2. Typical longitudinal wave speed signature along the length of the FGM strip.

Now, by eliminating the parameter W_f in Fig. 3, a "look-up chart" for correlating E_{static} with the measured wave speed C_1 can be established and this

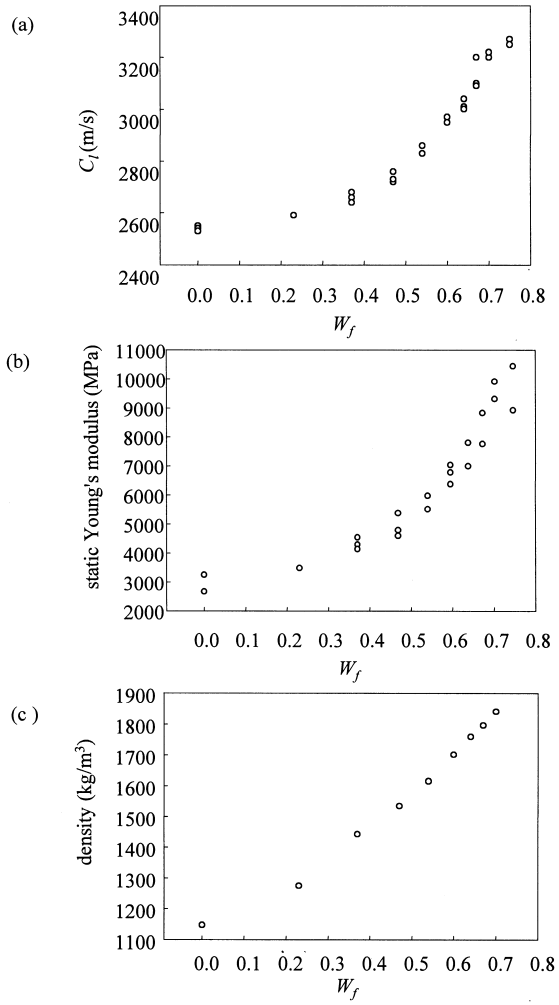

Fig. 3. Measured characteristics, namely, (a) longitudinal wave speed, (b) static Young's modulus and (c) average density of homogeneous particulate compositions as a function of weight fraction of the filler material.

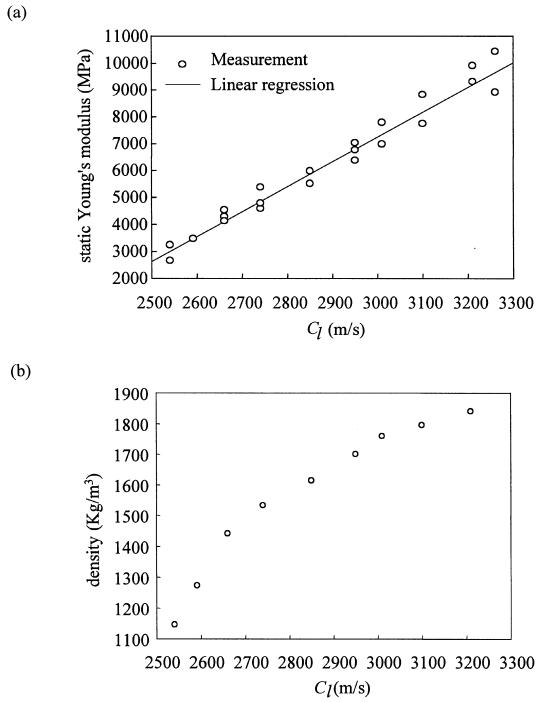

Fig. 4. Measured characteristics, namely, (a) static Young's modulus, (b) average density of homogeneous particulate compositions as a function of longitudinal wave speed measurements.

is shown in Fig. 4(a). A regression analysis of the data suggests an approximately linear relationship between the measured values of E_{static} and C_1 over the range of the weight fractions used in this study. Similarly, one can obtain a corresponding relationship between the density and wave speed, as shown in Fig. 4(b).

Next, the calibration chart shown in Fig. 4(a) was used to determine the spatial variation of Young's modulus in the FGM (Fig. 2) strip discussed earlier. Knowing the correspondence between the quasi-static values of Young's modulus and wave speeds, the variation of the Young's modulus in the cast FGM is determined and is plotted in Fig. 5. Thus, the ratio of the Young's moduli

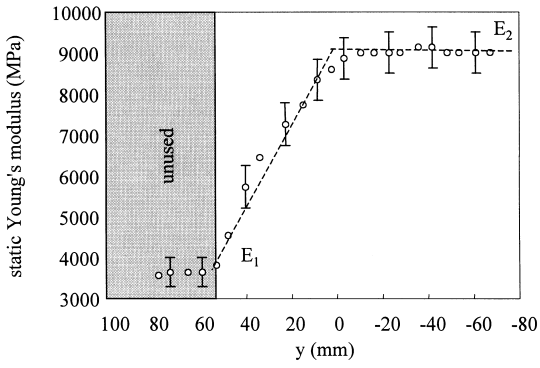

Fig. 5. Variation of static Young's modulus as a function of the position along the length of the gravity cast FGM.

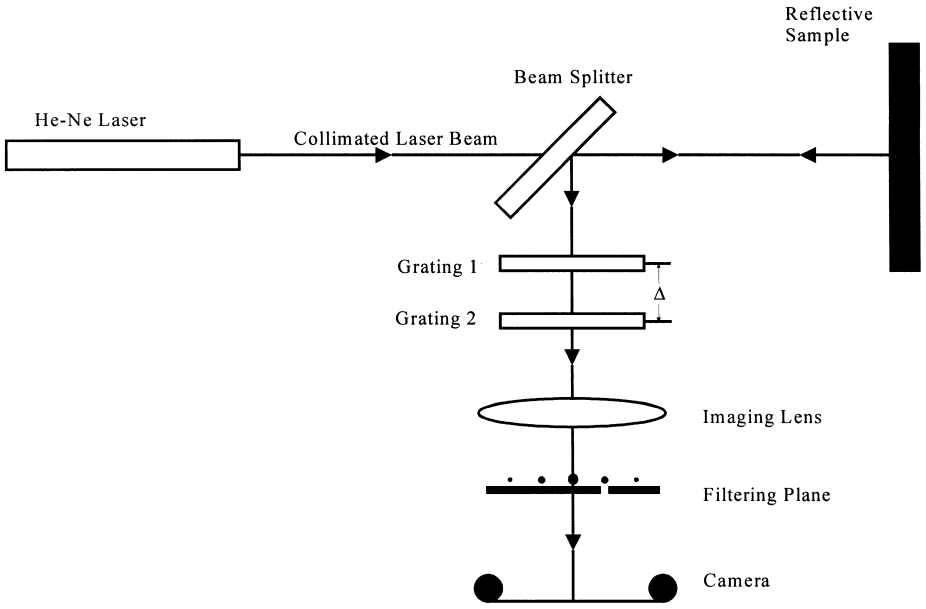

Fig. 6. CGS optical set-up used for mapping crack tip deformations in FGMs.

between the ends of the FGM interlayer is approximately 1:3 for the casting shown in Fig. 2. The dotted lines represent the linear fit of the Young's moduli corresponding to the various sections of the sample. The epoxy-rich region, shown shaded in Fig. 5, was not used in our subsequent fracture experiments.

For the sake of completeness, by using the material density and wave speed data shown in Fig. 4(b), the dynamic values of Young's modulus (E_{dyn}) for the FGM were also obtained and the details are reported in Appendix A. A linear relationship between the two quantities is evident. By comparing Fig. 4(a) and Fig. 10, a modest loading rate dependency of the material becomes apparent. As expected, higher values of the Young's modulus under dynamic conditions can be seen, with dynamic (solid line) to static (broken line) moduli ratios of 1.65 and 1.3, for the pure epoxy and the samples with the highest glass concentration, respectively. Evidently, the rate dependent behavior is somewhat higher for pure epoxy when compared to the ones that have substantial weight fraction of glass beads. *It should be noted, however, that* E_{dyn} *measurements are not used in the present work.*

3. OPTICAL MAPPING OF CRACK TIP DEFORMATIONS

The optical method of reflection Coherent Gradient Sensing (CGS) [16] was used to examine the surface deformations in the crack tip region when the sample was subjected to symmetric three-point bending. In the current study, the gradients of the out-of-plane displacements $w(x,y)$ with respect to the x-coordinate were measured. The FGM sample whose Young's modulus variation is shown in Fig. 5 was machined flat and a thin layer of epoxy (a few micrometers thick) was deposited and cured while sandwiching between an acrylic disk. This produces a flat, specular surface necessary for measuring the gradients of out-of-plane deformations in real-time. Subsequently, an edge notch of width 150 μm and length 6 mm ($a/W = 0.25$) was cut into the specimen near the interface between the graded and the homogeneous halves ($y = 0$).

The plan of the optical set-up for reflection CGS is shown in Fig. 6. A collimated beam of light (planar wave front) is incident on the sample surface through a beam splitter. The reflected beam or the object wave front carries the information about the non-planarity of the surface produced as a result of the surface deformations near the crack tip. The angular deflections of the light rays relative to the optical axis are then measured as interference patterns by a wave front shearing apparatus consisting of two Ronchi (rectangular profile) gratings of identical pitch with grating lines parallel to the y-direction for wave front shearing in the x-direction. The gratings are separated along the optical axis by a distance Δ. The gratings shear the wave front laterally in discrete directions depending on the grating pitch and the wavelength of the light used. These wave fronts are collected by an imaging lens of a camera and diffraction spots are displayed on the back focal plane of the lens. By filtering at either ± 1 diffraction spots, the fringe patterns representing contours of constant $(\partial w/\partial x)$ can be imaged. The details of the technique and mathematical basis for the field equations are reported in Tippur *et al.* [16]. The governing equation relating the deformations and the experimental parameters in this

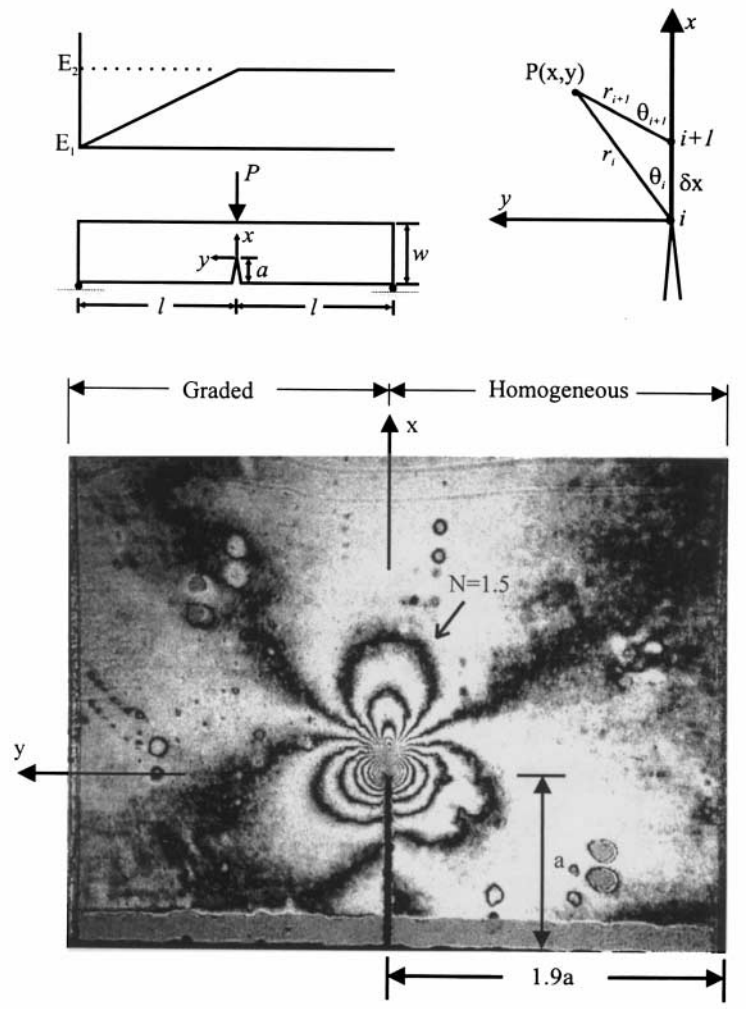

Fig. 7. Crack tip interference patterns representing $\delta w/\delta x$ contours (a = 5.5 mm, $2l$ = 102 mm, w = 24 mm and notch width = 150 μm).

case are

$$\frac{\partial w}{\partial x} = \frac{Np}{2\Delta}, \quad N = 0, \pm 1, \pm 2, \ldots \tag{1}$$

where N denotes the fringe orders, p the grating pitch ($=25\,\mu$m) and Δ the grating separation distance ($\approx$43 mm). A fringe pattern obtained from a three-point-bending experiment with an edge crack in the FGM discussed earlier (Fig. 5) is shown in Fig. 7 along with the specimen configuration. Here the crack was located where the FGM makes a smooth transition to the constant modulus region of $E = E_2$. The sensitivity of the fringes is approximately 0.008° per half-fringe. Although the loading configuration is symmetric, the fringes show modest global asymmetry about the crack plane as a result of the elastic gradient in $y > 0$. However, as one approaches the crack tip ($r \longrightarrow 0$), the fringe asymmetry seems to diminish indicating a rather small mode-mixity. (If each of the fringe lobes in these tri-lobed patterns rotates by 60°, a transition from pure mode-I to mode-II arises in homogeneous materials [16].) This could potentially be due to a rather slow variation of the modulus over the length of the specimen (half span = 51 mm).

4. FRACTURE PARAMETER ESTIMATION FROM INTERFERENCE FRINGES

Next, the optical measurements are used to extract fracture parameters in the FGM. The representation of the fringe patterns as derivatives of out-of-plane displacements is reasonable for small shearing distances [equation (1)]. The wave front shearing distance in this case being approximately 1 mm, a difference representation instead of a derivative representation is more appropriate. Other optical investigations on homogeneous fracture specimens in recent years have successfully used a difference interpretation for analyzing the CGS

fringes [17]. Accordingly, equation (1) is modified as

$$\frac{\partial w}{\partial x} \approx \frac{\delta w}{\delta x} = \frac{w_{i+1} - w_i}{\delta x} = \frac{Np}{2\Delta} \tag{2}$$

where $\delta(\cdot)$ represents the difference operator.

To extract the fracture parameters from fringe patterns, existing plane stress crack tip models were used. Using eigenfunction analysis, Eischen [18] has shown that the crack tip stresses in an FGM have the standard $\sqrt{r}$ singularity as in a homogeneous material. However, at the moment, explicit asymptotic field equations for cracked FGMs with general elastic property gradients are unavailable. Only the dominant terms in the crack tip stresses have been reported by Erdogan [8]. When a unidirectional shear modulus variation of the form $\mu(y) = \mu_1 \exp(\gamma y) \equiv \mu_1 \Phi(y;\mu)$ where $\gamma = (1/l)\log(\mu_1/\mu_2)$ is prescribed *perpendicular* to the crack orientation, the dominant terms in the crack tip stress field in FGMs are shown to assume the form [8]

$$\sigma_{\alpha\beta}(r,\theta) \cong \frac{\Phi(y;\mu)}{\sqrt{2\pi r}}(K_{\mathrm{I}} f^{\mathrm{I}}_{\alpha\beta}(\theta) + K_{\mathrm{II}} f^{\mathrm{II}}_{\alpha\beta}(\theta)), \quad \alpha,\beta = x,y. \tag{3}$$

equation (3) further reduces to the well-known homogeneous counterparts in the limit $r \longrightarrow 0$ [8, 13]:

$$\sigma_{\alpha\beta}(r,\theta) \cong \frac{1}{\sqrt{2\pi r}}(K_{\mathrm{I}} f^{\mathrm{I}}_{\alpha\beta}(\theta) + K_{\mathrm{II}} f^{\mathrm{II}}_{\alpha\beta}(\theta)), \quad \alpha,\beta = x,y \tag{4}$$

where $f(\theta)$ are the universal angular functions and $\sigma_{\alpha\beta}$ the stress components.

In the current work, the experimental modulus variation $E^{\mathrm{expt}}(y)$ in the FGM can be approximated by a linear function (broken line in Fig. 5) as

$$E^{\mathrm{expt}}(y) = E_2 \Phi^{\mathrm{expt}}(y,E) \equiv E_2\left(1 - \frac{\delta E}{E_2}\left(\frac{y}{l}\right)\right) \tag{5}$$

where $\delta E = (E_2 - E_1)$ and l ($\cong$51 mm) is the half-span of the beam. Therefore, *by conjecture* [19], equation (3) can be modified for analyzing the optical data as

$$\sigma_{\alpha\beta}(r,\theta) \cong \frac{\Phi^{\mathrm{expt}}(y;E)}{\sqrt{2\pi r}}(K_{\mathrm{I}} f^{\mathrm{I}}_{\alpha\beta}(\theta) + K_{\mathrm{II}} f^{\mathrm{II}}_{\alpha\beta}(\theta)). \tag{6}$$

The fringe pattern shown in Fig. 7 was analyzed based on the approximation that *K*-dominant behavior prevails in the near vicinity of the crack tip [equation (6)]. *In a number of previous optical investigations on homogeneous* [16] *and bimaterial* [20] *fracture specimens, it has been shown that plane stress conditions take hold beyond a radial distance of approximately* $r/B \geq 0.3$–0.5 (B being the specimen thickness) *depending on the angle* θ. Hence, it is reasonable to assume a plane stress approximation in the FGM sample also at similar distances. For plane stress conditions, the crack tip out-of-plane displacements are related to the normal stresses as

$$\varepsilon_z \cong \frac{2w}{B} = -\frac{\nu}{E}(\sigma_x + \sigma_y) = -\frac{\nu\Phi^{\mathrm{expt}}(y;E)}{E^{\mathrm{expt}}(y)\sqrt{2\pi r}}(K_{\mathrm{I}} g^{\mathrm{I}}(\theta) + K_{\mathrm{II}} g^{\mathrm{II}}(\theta)) \tag{7}$$

where $g^{\mathrm{I,II}}(\theta) = f^{\mathrm{I,II}}_{xx}(\theta) + f^{\mathrm{I,II}}_{yy}(\theta)$. Then we can write the relationship between the optical measurements and the crack tip field as ($r \longrightarrow 0$)

$$-\frac{\nu B}{(\delta x)E_2\sqrt{2\pi}}\left[K_{\mathrm{I}}\left\{\left(r^{-1/2}\cos\frac{\theta}{2}\right)_{i+1} - \left(r^{-1/2}\cos\frac{\theta}{2}\right)_i\right\} - K_{II}\left\{\left(r^{-1/2}\sin\frac{\theta}{2}\right)_{i+1} - \left(r^{-1/2}\sin\frac{\theta}{2}\right)_i\right\}\right] = \frac{Np}{2\Delta}. \tag{8}$$

In the above, $r_{i+1} = \sqrt{(x - \delta x)^2 + y^2}$ and $\theta_{i+1} = \tan^{-1}[y/(x - \delta x)]$. Interestingly, in view of the *K*-dominant assumptions, for the field quantity under consideration modulus variation drops out leaving behind the crack tip modulus ($E(y = 0) = E_2$) in equation (8) implying a locally homogeneous behavior ($r \longrightarrow 0$) in the near tip vicinity of a mixed-mode crack.

The optical data was digitized around the crack tip to extract the fringe location (r,θ) and fringe order (N) information. A least-squares analysis was used to extract the fracture parameters from the experimental data by minimizing the function $\sum_{j=1}^{m}[F(r,\theta;K_{\mathrm{I}},K_{\mathrm{II}}) - (Np/2\Delta)]_j^2$ with respect to the unknown coefficients K_{I} and K_{II}. Here m denotes the total number of data points used in the analysis and function F is the left-hand side of equation (8). Other details of the analysis are similar to the ones used in the homogeneous counterparts (see, e.g. Refs [17, 21]) and are not repeated in favor of brevity. *Some restrictions on the data set had to be imposed to ensure that the data used in the analysis come from regions where plane stress behavior is known to prevail.* It is well known that the crack tip vicinity undergoes three-dimensional deformations where two-dimensional solutions become inadequate [16]. The size of this zone around a mode-I crack tip is known to extend up to approximately one half plate thickness distance ($0.5B$) ahead of the crack and to a smaller extent (up to about $0.3B$), in the region behind the crack tip ($90^\circ < \theta < 135^\circ$) for a mode-I crack in a homogeneous material [16]. Thus, in the case of the FGM, the region $90^\circ < \theta < 135^\circ$ and $0.4 < r/B < 0.7$ (or, 2.2 mm $< r <$ 4.0 mm) was identified as the region most suitable for data analysis based on the *K*-dominant assumption yet outside the zone of sub-

Table 2. Comparison of measured and computed fracture parameters for FGM crack (P = 350 N, a = 6.0 mm, $2l$ = 102 mm, w = 24 mm and notch width = 150 μm)

	$\|K\|$ (MPa m$^{1/2}$)	ψ (deg)	Remarks
Optical measurements	2.19 ± 0.2	3.6 ± 1	Least-squares analysis using equation (8)
FEA results	2.18	0.3	Contour integral around the crack tip at $r/B = 0.2$; $E = E_2$
Boundary collocation	2.20	0.0	Homogeneous; $E = E_2$

stantial three-dimensional effects. The outer limit of the analysis is dictated by the diameter of the ultrasonic transducer (~4 mm) over which the material behavior can be assumed to be homogeneous. Results from the least-squares analysis of the optical data are presented in Table 2. Evidently, the crack tip is undergoing a predominantly mode-I deformation as a result of the loading configuration and a slow spatial variation of the modulus.

At the moment, for the chosen specimen configuration, fracture parameters are not reported in the literature. Hence, an independent finite element analysis of the experiments was carried out. Plane stress elastostatic finite element simulations were carried out using the MSC/NASTRAN™ software package. The mesh discretization used in this investigation is shown in Fig. 8. It consisted of 8700 rectangular eight-node isoparametric elements with the finest mesh (smallest element size 300 μm) limited to the central region of the sample. (The FE model was calibrated against homogeneous and bimaterial solutions for the geometry reported in the literature. The details of the same are avoided here for brevity.) The choice of the rectangular mesh was to enable column-wise increments in the elastic properties to simulate the FGM. *The Young's modulus variation corresponding to the one shown in Fig. 5 (broken line) was applied to the individual columns of elements while keeping the Poisson's ratio constant*. The J-integral was computed using this model at a small distance $r/a \sim 0.2$ mm away from the crack tip and subjected to mode-partitioning to determine the stress intensity factors by invoking the assumption of homogeneous material behavior ($E = E_2$) in a small region close to the crack tip. (It should be noted that when the elastic properties vary in the direction perpendicular to the crack, the J-integral is path independent [22, 15].) For comparison purposes, the value of K_I for a homogeneous three-point beam with $E = E_2$ is also included.

Evidently, the optical estimation of $|K|$ is in fairly good agreement with the ones from the FEA results. The measured values of mixity ψ ($= \tan^{-1}(K_{II}/K_I)$), however, show a smaller amount of asymmetric deformation. This is due the differences in the regions where the data is collected in the two instances. A relatively smaller contour of integration around the crack tip where the assumption of homogeneous material behavior holds better is used in estimating the FEA results. On the other hand, the optical data come from regions relatively far away from the crack tip compared to the ones used for finite element computations, thereby weak-

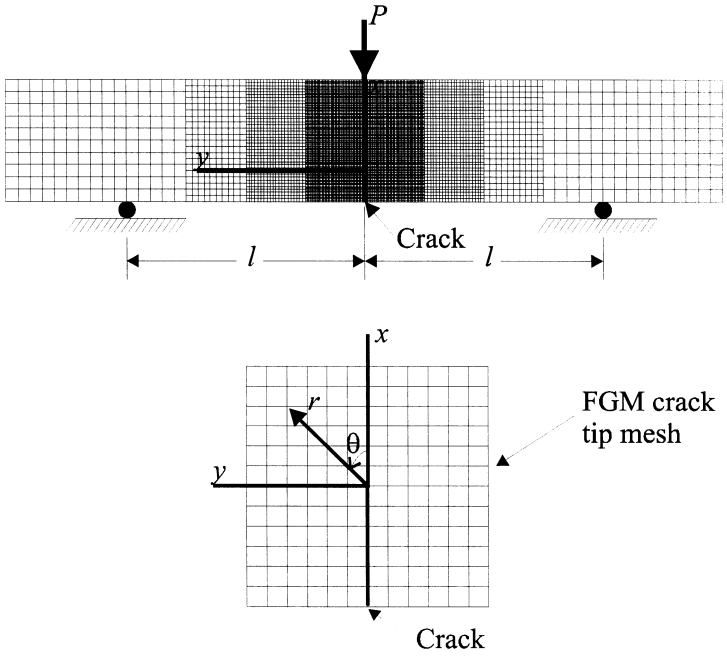

Fig. 8. Finite element mesh used in the simulations of symmetric three-point bending.

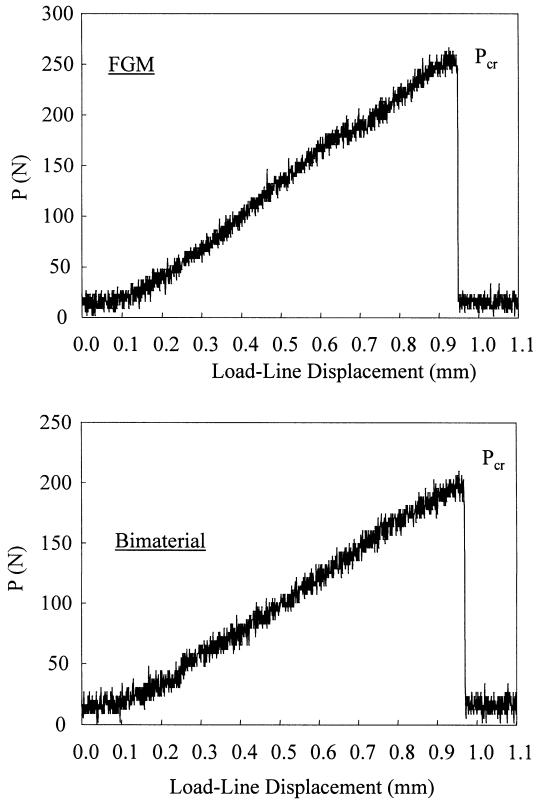

Fig. 9. A typical load vs load-line displacement plot from three-point-bending fracture tests.

ening the assumptions of K-dominance used in the least-squares analysis. In view of the ever present three-dimensional deformations in all experimental situations with finite specimen sizes, exclusion of the data in close vicinity of the crack tip is inevitable. Thus, the experimental data have to be invariably derived from finite distances. Hence, a full-field asymptotic description for cracked FGMs would be of great value for improving the fracture parameter estimation and a subsequent development of a fracture criterion and verification.

5. FRACTURE TESTS

The literature suggests favorable fracture performance of FGMs relative to bimaterials of the same Young's modulus mismatch. However, quantitative test results demonstrating the same are rather sparse at the moment. Tests to verify this were carried out through crack initiation tests using FGM, bimaterial and homogeneous samples ($a/W = 0.25$, $B = 6$ mm). In order to achieve consistency in the modulus gradient in the FGMs between samples in multiple tests, an FGM sheet was cast instead of individual strips as described earlier. Sharp cracks (disbonds) were introduced into the samples by bonding the FGM sheet to a homogeneous ($E = E_2$) sheet with debonds at discrete locations using commercially available Teflon tape of thickness 30–50 μm. *The epoxy–glass mixture with the same weight fraction of the filler material used for casting the homogeneous* ($E = E_2$) *sheet was used to bond the two sheets*. Using a similar procedure, homogeneous sheets of $E = E_2$, and a bimaterial sheet obtained by bonding homogeneous sheets of modulus E_1 and E_2, all with similar disbonds were prepared. This method of introducing discontinuities into the samples was preferred since straight crack fronts could be produced in multiple samples consistently. Subsequently, edge cracked beam samples were machined from these sheets. The samples were subjected to quasi-static three-point bending (span 89 mm, width 20 mm) and load–displacement data were acquired as the samples were loaded monotonically (cross-head velocity of 2 mm/min) in a displacement controlled loading device. Samples of load vs load-line displacement responses for FGM and bimaterial specimen tests are shown in Fig. 9 and in each case a distinct peak (P_{cr}) followed by a sudden drop in the load corresponding to crack initiation can be seen. The non-linearity in the initial part of the response is due to the slack in the loading fixtures and the rest of the loading history until fracture is essentially linear. In each of the experiments the crack growth occurred along $\theta = 0^\circ$ as a result of the plane of weakness along the bond line. The crack initiation load was used to compute the J-integral using the finite element analysis wherein the measured Young's modulus variations were used. By invoking the equivalence of the energy release rate G and the J-integral, the results are tabulated in Table 3. Also included in the table are the stress intensity factors at crack initiation for homogeneous and FGM samples.

The test results are based on *three test samples in each category*. The data clearly demonstrate the improvement in the fracture performance of FGMs relative to the bimaterial counterparts. When compared to the bimaterial samples, the fracture load of the FGM and hence the product of the critical value of the energy release rate and the crack tip Young's modulus ($E(x,y = 0) = E_2$ for the FGM

Table 3. Fracture performance of FGMs, bimaterials and homogeneous samples (a = 5 mm, $2l$ = 89 mm, w = 20 mm and notch width ~ 50 μm)

	P_{cr} (N)	$G_{cr}E(x,y = 0)$ ($\times 10^{10}$ N^2/m^3)	K_I, K_{II} (MPa m$^{1/2}$)
FGM	245.3 ± 5	212.4	1.46, 0.04
Homogeneous ($E = E_2$)	254.2 ± 15	234.9	1.53, 0
Bimaterial	196.2 ± 5	149.0	—

and homogeneous beam and $E(x,y=0) = 2E_1E_2/(E_1+E_2)$ for the bimaterial) is higher by a factor in excess of 1.4. *The improvement in the fracture performance observed here is rather conservative since we have used bonding to join the FGM to the homogeneous material. In reality, the virgin FGM with a smooth transition from one modulus to the other would provide a higher fracture toughness*. The results obtained from the FGM tests closely follow those of the homogeneous samples with $E = E_2$.

6. CONCLUSIONS

Preparation, elastic characterization, crack tip field measurements and fracture tests of a functionally graded material were undertaken. A graded particulate composition comprising of spherical glass filler particles in an epoxy matrix was developed using the gravity casting technique. A method of measuring the Young's modulus variation in the FGM is developed and a "look-up" chart relating the quasi-static values of the measured Young's modulus and measured longitudinal wave speed are provided. An FGM with an approximately linear Young's modulus variation $E_1{:}E_2 \approx 1{:}3$ was realized. Subsequently, full-field optical measurement of crack tip deformations in the FGM was carried out for the case when an edge crack is situated near the interface of the FGM and homogeneous substrate of equal thickness. A method of extracting the fracture parameters from measured CGS interference data using *K*-dominant behavior is developed. Satisfactory results were obtained in the measurement of the magnitude of the stress intensity factor. Also, the need for explicit asymptotic crack tip fields which take into account Young's modulus gradient over finite distances from the crack tip has been emphasized to further improve the accuracy of the estimation process. Relative fracture performance of FGM beam samples undergoing symmetric three-point bending was explored by conducting failure tests. The breaking loads for FGM samples were significantly higher than those for the bimaterial and were approximately the same as the homogeneous samples when the crack is located at the interface of the FGM and homogeneous substrate. Using breaking loads as input in finite element simulations fracture parameters have been computed and they clearly favor FGM when compared to the bimaterial counterparts.

Acknowledgements—The support for parts of this research by NSF Mechanics and Material Program (CMS9622055) and ARO Solid Mechanics Program (DAAG55-97-1-0110) is gratefully acknowledged.

REFERENCES

1. Marple, B. S. and Boulanger, J., *J. Am. Ceram. Soc.*, 1994, **77**(10), 2747.
2. Fukui, Y., Takashima, K. and Ponton, C. B., *J. Mater. Sci.*, 1994, **29**, 2281.
3. Abboud, J. H., Rawlings, R. D. and West, D. R. F., *Mater. Sci. Technol.*, 1994, **10**, 414.
4. Sampath, S., Gausert, R. and Herman, H., *J. Metals*, 1995, **47**, 30.
5. Atkinson, C. and List, R. D., *Int. J. Engng Sci.*, 1978, **16**, 717.
6. Gerasoulis, A. and Srivastav, R. P., *Int. J. Engng Sci.*, 1980, **18**, 239.
7. Erdogan, F., *Tr. J. Engng Env. Sci.*, 1994, **18**, 185.
8. Erdogan, F., *Composites Engng*, 1995, **5**(7), 753.
9. Ozturk, M. and Erdogan, F., *ASME J. appl. Mech.*, 1993, **60**, 406.
10. Chen, Y. F. and Erdogan, F., *J. Mech. Phys. Solids*, 1996, **44**(5), 771.
11. Giannakopoulos, A. E., Suresh, S., Finot, M. and Olsson, M., *Acta mater.*, 1995, **43**, 1335.
12. Choules, B. D. and Kokini, K., *ASME J. Engng Mater. Technol.*, 1996, **118**, 522.
13. Jin, Z.-H. and Batra, R. C., *J. Mech. Phys. Solids*, 1996, **44**(8), 1221.
14. Bao, G. and Cai, H., *Acta mater.*, 1997, **45**(3), 1055.
15. Gu, P. and Asaro, R. J., *Int. J. Solids Struct.*, 1997, **34**(24), 3085.
16. Tippur, H. V., Krishnaswamy, S. and Rosakis, A. J., *Int. J. Fract.*, 1991, **52**, 91.
17. Tippur, H. V. and Xu, L., *Strain*, 1995, **31**(4), 143.
18. Eischen, J. W., *Int. J. Fract.*, 1987, **34**, 3.
19. Erdogan, F., Private communications, 1998.
20. Sinha, J. K., Tippur, H. V. and Xu, L., *Int. J. Solids Struct.*, 1997, **34**(6), 741.
21. Ramaswamy, S. and Tippur, H. V., *Exp. Mech.*, 1993, **33**(3), 243.
22. Rice, J. R., *ASME J. appl. Mech.*, 1968, **35**, 379.
23. Marur, P. R. and Tippur, H. V., *ASTM J. Testing Eval.*, to appear.

APPENDIX A

It is well known that the longitudinal wave speed is related to the elastic constants as

$$C_l = \sqrt{\frac{E_{\text{dyn}}}{\rho}\frac{(1-\nu)}{(1-\nu)(1-2\nu)}}.$$

The plots in Figs 3(a) and (c) show that both the wave speed C_l and the density show parabolic variation relative

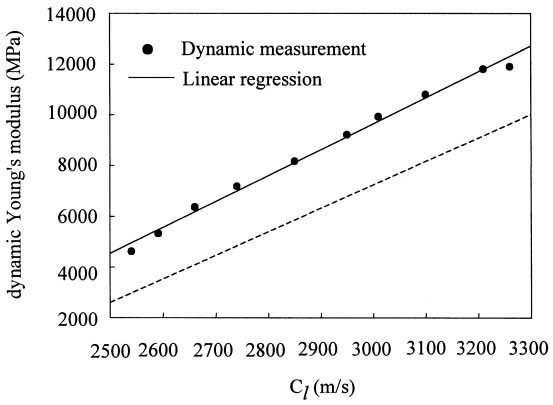

Fig. 10. Variation of dynamic Young's modulus (solid line) values for homogeneous particulate compositions as a function of the longitudinal wave speeds. (The broken line corresponds to the Young's modulus of the material under quasi-static loading conditions.)

to the weight fraction of the glass beads in the mixture. From a previous study [23] the values of the Poisson's ratio (v) is shown to have a narrow variation of 0.33–0.37 for this particulate composite. Hence, by assuming that the Poisson's ratio is approximately constant and equal to 0.35, and using the independently measured values of the material density, E_{dyn} was determined for each of the homogeneous specimens. The values of E_{dyn} thus obtained are plotted against the wave speed in Fig. 10. Again, a linear relationship between the two quantities is evident. By comparing Fig. 4(a) and Fig. 10, the loading rate dependency of the composite alluded to earlier becomes apparent. As expected, higher values of the Young's modulus under dynamic conditions can be seen, with dynamic (solid line) to static (broken line) moduli ratios of 1.65 and 1.3, for the pure epoxy and the samples with the highest glass concentration, respectively. Evidently, the rate dependent behavior is somewhat higher for pure epoxy when compared to the ones that have substantial weight fraction of glass beads.